Physical and mechanical characterization of concrete exposed to elevated temperatures by using ultrasonic pulse velocity

Caracterización física y mecánica de concreto expuesto a temperaturas elevadas usando velocidad de pulso ultrasónico

Ricardo Alfredo Cruz Hernández[1], Luis Eduardo Zapata Orduz[1], Luz Amparo Quintero Ortiz[2], Julián Orlando Herrera Ortiz[2]*

[1] Escuela de Ingeniería Civil, Facultad de Ingenierías Físico-Mecánicas, Universidad Industrial de Santander. Cra 27 calle 9. Bucaramanga, Colombia.

[2] Escuela de Ingeniería Metalúrgica y Ciencia de Materiales, Facultad de Ingenierías Físico-Químicas, Universidad Industrial de Santander. Cra 27 calle 9. Bucaramanga, Colombia.

(Received May 12, 2014; accepted April 06, 2015)

Abstract

Experimental investigations were carried out for assessing the influence of thermal loadings on the physical and mechanical properties of plain concrete after fire exposure. Cylindrical specimens were subjected to thermal loading at different temperatures inside a muffle furnace; while cubic specimens were exposed to direct flame following the ISO 834 standard curve. For both specimens' geometries the thermal loading was applied until it reached the selected temperature which was held for an hour. The specimens were tested for weight loss, optical microscopy, ultrasonic pulse velocity, residual compressive strength, X-ray diffraction and porosity. It has been observed that with the increase in the thermal loading, the physical and mechanical properties experienced significant detriment. The results suggested that the ultrasonic pulse velocity method is appropriate as an indicator of concrete compressive strength and microstructural properties after fire exposure.

----------*Keywords:* elevated temperature, concrete, compressive strength, ultrasonic pulse velocity

* Corresponding author: Ricardo Alfredo Cruz Hernández, e-mail: racruz@uis.edu.co
DOI: 10.17533/udea.redin.n75a12

Resumen

En el presente trabajo se reportan los resultados de experimentos llevados a cabo bajo cargas de fuego para evaluar las propiedades físicas y mecánicas en concreto sin reforzar. Especímenes cilíndricos fueron expuestos a diferentes temperaturas dentro de una mufla; mientras que especímenes cúbicos fueron expuestos a llama directa usando la curva estándar ISO 834. Las cargas térmicas se aplicaron hasta alcanzar una determinada temperatura la cual fue mantenida durante una hora. Los ensayos consistieron en pérdida de masa, microscopia óptica, velocidad de pulso ultrasónico, resistencia de compresión residual, difracción de rayos X y porosidad. Se observó que con el incremento de la temperatura las propiedades físicas y mecánicas experimentaron grandes daños. Los resultados mostraron que el método de la velocidad de pulso ultrasónico es apropiado para la evaluación de la resistencia a la compresión y las propiedades micro-estructurales del concreto después de ser expuesto a fuego.

----------*Palabras clave*: temperatura elevada, concreto, resistencia, velocidad de pulso ultrasónico

Introduction

The damage caused by building fires is a very important concern to the civil infrastructure. Furthermore, the non-destructive ultrasonic pulse velocity (UPV) method has been widely used in concrete works to study mechanical properties. The UPV consists in measuring the transit time of an ultrasonic pulse through the material. The extensive acceptance of UPV in concrete can be summarized as follows: (i) it is easy to use; (ii) the results can be quickly achieved *in situ*, and (iii) the possibility to relate UPV measurements with physical and/or mechanical properties of concrete [1]. Usually to conduct fire studies in concrete structures, idealized fires can be considered. The most widely used test specifications are the well-known standard fire given in ISO 834 [2], the ASTM E119 [3], and parametric fires given in the Eurocode [4]. Therefore, in a section of this paper, fire temperature, T, is considered as the temperature developed from the fire temperature (T)-time (t) profile from the ISO 834 standard curve (Eq. 1).

$$T = 345\ log_{10}(8t+1) + T_o \qquad (1)$$

In Eq. 1 t is the time (min) and T_o is the room temperature (°C). The ISO-curve has been widely used in works using fire on concrete. Nevertheless, the artificial fire loading (i) present a theoretical basis, (ii) is assumed in the whole compartment, and (iii) the temperature never goes down. However, there are a significant number of studies on concrete components exposed to fire. These works have been focused on different topics of this important scientific area, for example in [5] estimating the reliability of a fire-exposed concrete tunnel. Another study [6] investigated reinforced concrete beams exposed to fire. In [7] assessed the influence of thermal loading on compressive strength of normal/high-strength concrete with/without polypropylene fibers. In [8] studied the effect of temperature on physical-mechanical properties of concrete containing silica fume. In a similar fashion, [9, 10] compared the mechanical properties of normal/high-strength concrete and evaluated the behavior of concrete exposed to high temperatures under different test conditions. In summary, the present work evaluates some physical and mechanical properties of plain concrete after fire exposure using UPV and optical microscopy analyses.

Materials and methods

Casting process

The raw materials used to the development of the experimental specimens, consisted of: 2.6 specific gravity (SSD) sand with 2.9% absorption and 2.8 fineness modulus. The coarse aggregate was 19 mm maximum size, 2.7 of specific gravity (SSD), and 0.6% absorption. Both, fine and coarse aggregate were igneous-metamorphic materials extracted from Pescadero (Santander, Colombia). The test specimens are composed of concrete samples cast at water-to-cement ratio of 0.5. The proportion (kg/m^3) for the concrete composition was as follows: 404 of cement, 202 of water, 944 of coarse aggregate and 809 of fine aggregate. There were two types concrete of samples: (1) cylindrical molds of 100 mm of diameter and 200 mm of height (ASTM C470) [11] and (2) 200x200x200 mm cubic (DIN EN 206-1:2001-07) [12]. Experimental samples were cast and cured during 28 days at 20-23 °C and 100% of relative humidity. After 28 days of curing, the samples were dried at ambient temperature before any test was conducted. Two K-type thermocouples were introduced during the casting process of the cubic specimens (Figure 1a). The thermocouples were fixed at 40 and 100 mm from the bottom with 40 mm of separation between them (Figure 1b).

Physical and mechanical tests

The methodology and techniques used to conduct the physical and mechanical tests can be described as follows: once the samples reached 28 days of curing, they were exposed to air dry conditions for 15 days and the following tests were conducted: compression tests (ASTM C39) [14] by using a Universal Testing Machine (400 kN in capacity), thermal loading as per ISO 834 [2], XRD (Brucker D8 Advanced with Da Vinci geometric) for mineralogical composition, optical microscopy (using Olympus SZ stereoscopy) for microstructural analysis, UPV conforms to NTC 4325 [15] by using a Pundit Plus (transducers 54 kHz), visual inspection, weight loss and porosity. These latter by using a balance Shimadzu BW22KH (maximum capacity 22 kg and error of 0.1 gram). With the exception of thermal loading, these tests were used before and after the fire exposure to develop comparative procedures. The optical microscopy technique was conducted on the cylindrical samples, which were cut into three slides as shown in Figure 2a, and the central portion of the specimen was used in the microscopy analysis (Figure 2b).

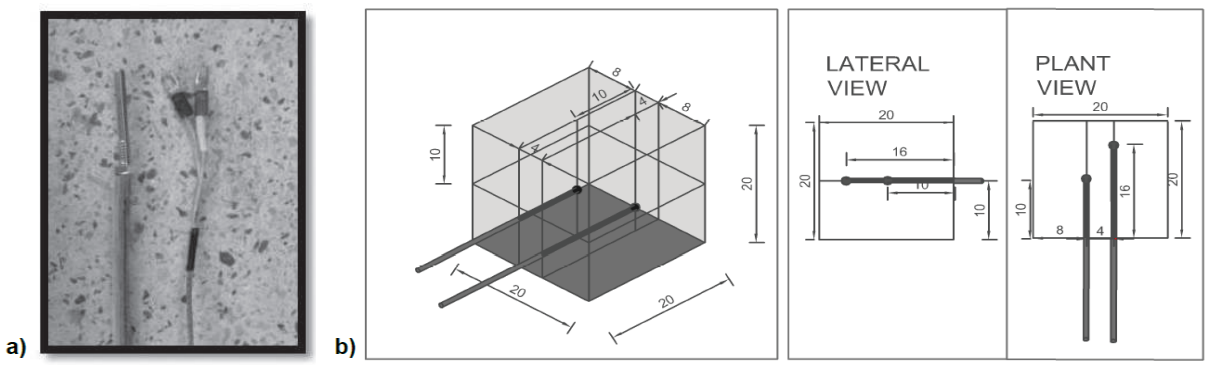

Figure 1 (a) K-type thermocouple. (b) Schematic of cubic specimen with thermocouples (dimensions in cm) [13]

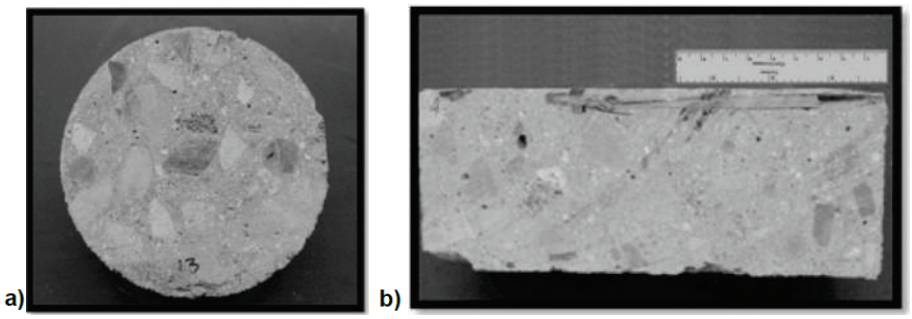

Figure 2 Sample preparation for optical microscopy (a) cross-section and (b) transverse view of cylindrical specimens [13]

The same procedure was applied in the control samples. For each interfacial zone (aggregate-cement paste), the area on the optical microscopy was digitally magnified approximately 17-fold. The porosity tests were conducted on the basis of Eq. 2 as follows: (i) the original cubic/cylindrical specimen is weighed in dry condition; (ii) the samples are weighted in water condition (sank), and (iii) after 24 hours of water condition the weight is registered.

$$P = \left(\frac{H-D}{H-S}\right) x\ 100\% \qquad (2)$$

Where P is the porosity in percentage (%), H is the mass in grams of the specimen in the wet state after 24 hours, D is the dry mass in grams, S is the mass of the sample in the immersed state. The UPV test used was the direct transmission method (Figure 3). The UPV measurements were recorded perpendicularly to the heat flow because the aim was to investigate the damage caused by the temperature change of the samples. For that reason, several measurements were taken along the axial length of the specimen.

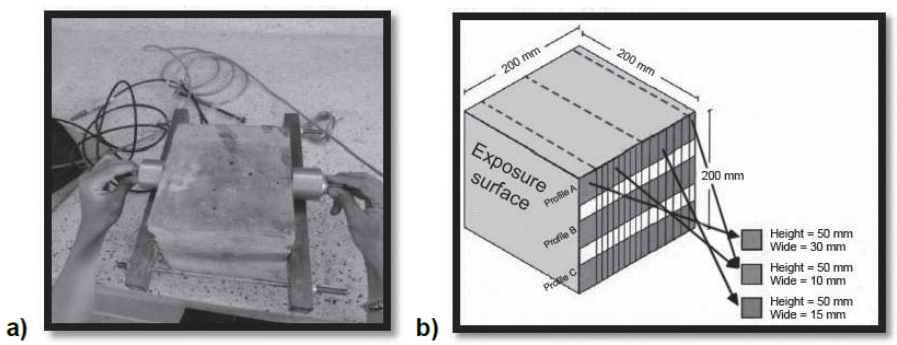

Figure 3 UPV (a) measurement in progress. (b) Schematic of the measurements in cubic samples [13]

Thermal loading

The fire exposure for cylindrical specimens was carried out in a muffle furnace equipped with thermocouples (up to 1200 °C). In the program 30 cylindrical specimens were employed and the temperatures were varied as follows: room temperature (non-exposed samples) (20 °C), 200, 400, 600, 800 and 1000 °C. In the developing of these tests six cylindrical and two cubical

samples were employed. Each temperature was maintained for an hour once it has been attained. The thermal loading was carried out following the ISO 834 standard curve, as shown later.

Results and discussion

The compressive strength of concrete is a vital requirement for structural and mechanical purposes. Nonetheless, other characteristics of concrete, such as durability may be more relevant in some specific or practical cases [16]. Therefore, the results of the present paper consisted of both types of analyses.

Visual inspection

Initial visual inspection revealed that all concrete specimens were smooth, grey-colored and without any visible crack or material deterioration. Figure 4 shows the sequence of the visual inspection in cylindrical samples as the temperature was increased. Material deterioration is often indicated by cracking and/or spalling on the concrete surface. At 200 °C the specimens did not exhibit damage on the surface. Changing in color from grey (T=20 °C) to yellow-pink was hardly visible. At 400 °C small cracks appeared on the surface (Figure 4b) and the pink color was barely evident when compared with samples at 200 °C. At 600 °C both the cracking pattern (Figure 4c) and the pink color are more evident than in the previous temperatures. At 800 °C the damage on the concrete surface is advanced due to pop-outs induced by dehydration phenomena pressures (Figure 4d) and so the color changed from grey to white at 20 °C. At 1000 °C the concrete samples experienced the worst surface damage because the aggregates were completely separated from the cement matrix and the samples could not be moved from the muffles due to their extreme fragility (Figure 4e).

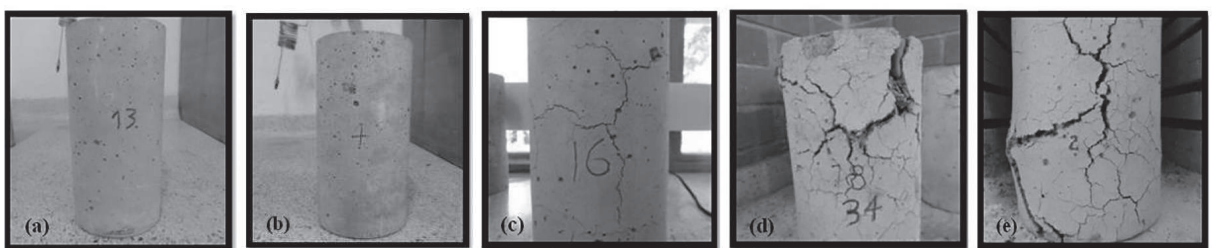

Figure 4 Surface appearance of the cylindrical specimens exposed to different temperatures (a) 200 °C, (b) 400 °C, (c) 600 °C, (d) 800 °C and (e) 1000 °C [13]

Figure 5 shows the effect of the temperature on cubic specimens which were heated following the ISO 834 standard curve (Eq. 1). The damage induced on cubic specimens was less severe than in the cylindrical samples. Figure 5a shows some soot on the exposed face, which is expected since the straight flame employed to reach 400 °C is characterized by its reduced O_2 content. As a result, uncompleted combustion is generated on the concrete surface with the corresponding soot-print. The presence of small cracks and pink color was also found on the surface of these samples. From Figure 5d it can be seen that there is no appreciable damage into the cut surface. In contrast, the cubic specimens exposed to 800 °C (Figs. 5b and 5e) exhibited a more severe deterioration than the previous one. At 1000 °C pop-outs started to appear because of the severe hot environment (Figs. 5c and 5f). Pop-out formation is related with expansions induced by dehydration phenomena and final damage in the concrete by tensile stresses. Systematic crack mapping as observed in Figs. 4(c-e) and 5(e-f) could be attributed to different thermal expansion coefficients between the aggregates and the cement matrix.

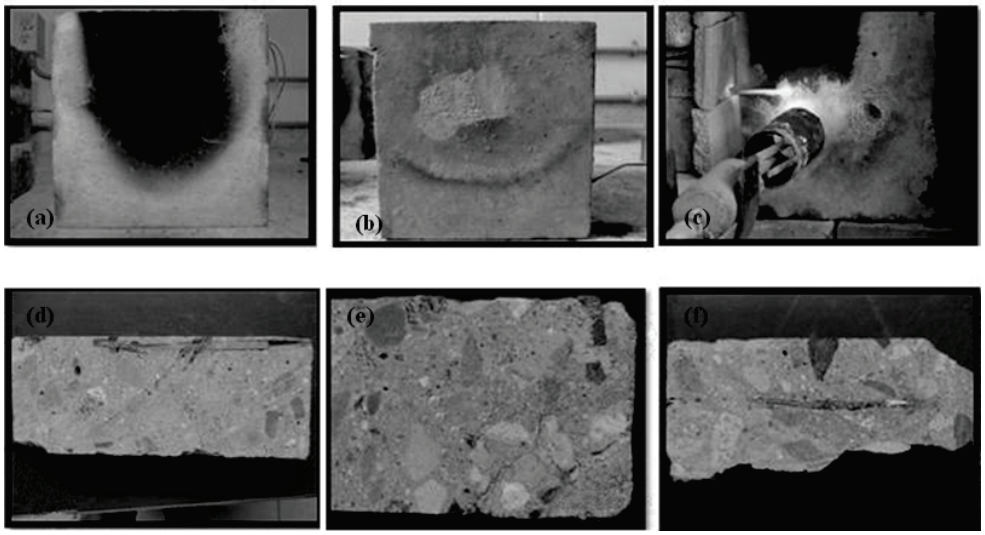

Figure 5 Cubic specimens exposed to different temperatures (a) 400 °C, (b) 800 °C, (c) 1000 °C and transversal sections of (d) picture a, (e) picture b and (f) picture (c) [13]

The ISO 834 standard curve was monitored in the cubic specimens by means of four thermocouples (Figure 1). Figure 6 shows the data collected on an experimental sample exposed at 1000 °C. The device placed on the exposed surface (called A) reached a temperature of 1000 °C; a second device located at 40 mm from the exposed surface (called B) reached a temperature of 265 °C; a third device located at 100 mm from the exposed surface (called C) reached 150 °C. An external thermocouple (called D) was employed to monitor the temperature of the chamber environment which registered a temperature of 70 °C during the experiments. Figure 6 shows the temperature behavior during the time of the described experiment. From Figures 5 and 6, it can be seen that the worst damage occurred on the exposed surface and it vanishes while the fire reached internal locations. Figure 6 shows that at the distance of typical cover (40 mm) for the steel bars in structural designs, they can reach temperatures of 140 °C at 2000 secs and 340 °C at 6000 secs of fire exposure as detected by the thermocouple B (in Figure 6 symbolized as Ther. B). Even at 100 mm from the exposed surface the temperature could reach 150 °C after 4000 *s* of fire exposure.

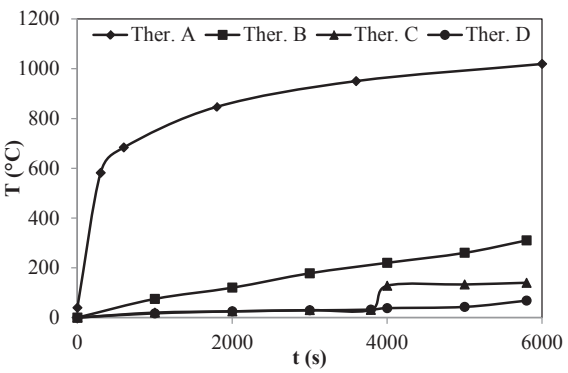

Figure 6 Temperature in cubic specimens as a function of time and thermocouple position

Optical microscopy

Figure 7 shows the crack formation with temperature increments. Significant color variations were observed at high temperatures as explained in the visual inspection section (Figure 4). Figure 7(a-b) showed that there are not significant differences between the interfacial zones at 200 °C compared with non-exposed concrete, in both type of samples a smooth surface without any crack formation in the interfacial transition zone is observed. On the other hand,

Figure 7c shows surface defects when compared to samples exposed at 200 °C and 400 °C. The smooth surface has now been replaced by a rough one and a series of holes were formed due to debonding of the coarse aggregates. Moreover, cracking formation was observed at both the cement mortar as well as in the interfacial zone between the coarse aggregate and the cement mortar, even some coarse aggregates suffered severe cracking. Finally, at 800 °C the cracking was more pronounced in the cement mortar, the interfacial zone and in some coarse aggregates.

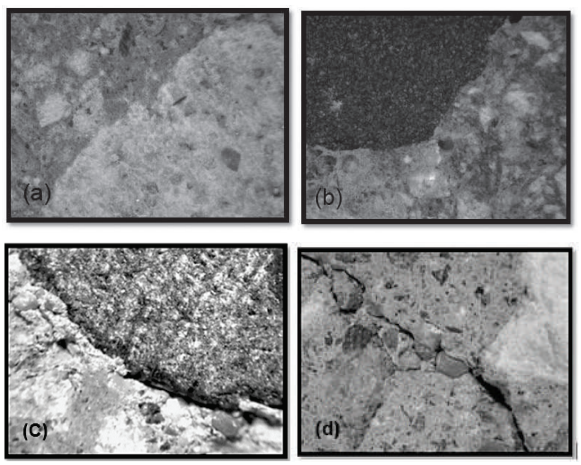

Figure 7 Aggregate-cement matrix zone (a) non-exposed, (b) 200 °C, (c) 600 °C and (d) 800 °C [13]

Weight loss

Figure 8 shows the average weight loss of three samples when the material is exposed to different temperatures. The reduction on weight of concrete specimens increased as the temperature was risen from 20 to 1000 °C for both samples types. Figure 8 reveals that in the range of 20-200 °C, the cylindrical specimens lost weight quickly due to evaporation of the free water, also elimination of the ettringite and gypsum is observed when comparing the XRD of samples exposed to fire against the control samples, this topic will be discussed when describing X-ray diffraction analysis. Within the temperature range of 200-600 °C, the weight is lost slowly because most of the water has been previously eliminated and the chemically combined water residuum is basically due to the elimination of the $Mg(OH)_2$ and $Ca(OH)_2$. At higher temperatures other mechanisms induced the damage in concrete such as decomposition of magnesium and calcium carbonates of the aggregates [17]. Furthermore, Figure 8 shows that the percentages of loss in weight (and the rate) for cubic specimens were lower than for cylindrical samples. This behavior is attributed to three reasons: (i) the cylindrical specimens experienced fire on their entire surface, while the cubic specimens were exposed to fire on one face only; (ii) the volume of the cubic specimens was 4.9 times bigger than the cylindrical ones and (iii) the cubic specimens were exposed to fire following the ISO 834 curve, while the cylindrical specimens were heated using a muffle system. Due to this latter heating method is slower than the proposed at ISO 834 approach, the cylindrical specimens had to be exposed more time to reach each selected temperature.

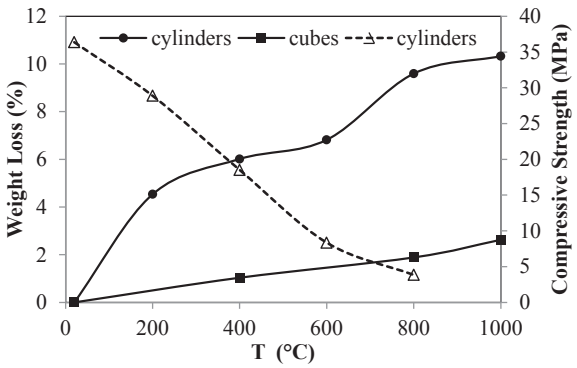

Figure 8 Compressive strength (dash line) and weight reduction (solid lines) as a function of fire exposure

Relationship between the ultrasonic pulse and compressive strength

It is well known, that there is no a standard correlation between the UPV and the concrete compressive strength as it is influenced by many factors [18]. One of the main factors

that disturb the correlation is the nature of the aggregates [19]. Therefore, it is expected that the following UPV-compression equations would help the post-fire compressive strength behavior under the present experimental conditions, to be understood. Also, correlations between UPV with porosity and temperature were developed by means of regression analysis. The weight of the relationship was determined by the correlation coefficient (Eq. 3), and the validity of the model is determined by statistical significance (p-value).

$$r = \frac{\sum_{i=1}^{N}(s-\bar{s})(\psi-\bar{\psi})}{\sqrt{\sum_{i=1}^{N}(s-\bar{s})^2 \sum_{i=1}^{N}\left(\psi-\bar{\psi}\right)^2}} \qquad (3)$$

In Eq. 3 ψ represents the estimated UPV value from the regression model and *s* represents the measured value in the laboratory conditions. The average values are represented by a hat symbol for both cases. From laboratory tests a regression analysis between the average of six UPVs (*V*) in m/s and three cylinders compression values (*C*) in MPa were performed, obtaining a correlation coefficient equal to 0.9985 by using a quadratic model (Eq. 4) which is the best fitted for the relationship under study. An *r*-value of more than 0.80 indicates an excellent correlation between the fitted parameters. Furthermore, a p-value of 0.0001 was found; therefore, it is possible to argue that there exists a very strong statistical significance (p-value<0.05) between the variables analyzed. The average gradient between compressive strength and pulse velocity was 0.009 MPa·s/m. Gradients found in concretes which have not been exposed to thermal loadings usually range between 0.02-0.03 MPa·s/m [20]; whereas the gradient in the present research was found to be an order of magnitude lower than the typical values for non-exposed concrete. The gradient values are indicating significant differences in the UPV measurements performed on concrete exposed versus non-exposed to fire loads.

$$C(V) = 2E^{-6}\,V^2 + 0.0011V + 3.3593 \qquad (4)$$

Following to [21] for non-exposed concrete with a density of approximately 2400 kg/m^3 in Table 1 the relationship between UPV and compressive strength is shown. In the present work, an average value of 3944 m/s (UPV) was found in the non-exposed concretes; consequently the present concrete mixture can be classified as "good" quality concrete. The compressive strength at ambient temperature for the present concrete cylinders was of 36.4 MPa at 43 days (Figure 8). Unfortunately, due to the extreme degradation experienced by the cylindrical samples at T=1000 °C (Figure 4e) neither UPV nor compressive strength were possible to be carried out in those samples. This latter experimental result is in accordance with what was reported in reference [7]. In the present work the compression value (MPa) as function of temperature (°C) (Eq. 5) statistically followed a quadratic polynomial behavior with *r*-value=0.9958 and p-value=0.0003. In general, the relationship between cylindrical compressive strength and exposure temperature was found to be similar with other investigations [22].

Table 1 Qualitative classification of the quality of concrete on the basis of UVP [21]

UPV (m/s)	*Quality of concrete*
> 4500	excellent
3500 - 4500	good
3000 - 3500	doubtful
2000 - 3000	poor
< 2000	very poor

$$C(T) = 2E^{-5}\,T^2 - 0.0564T + 38.238 \qquad (5)$$

The loss in compressive strength is set down to internal damage stresses, crack growth and expansive pressures from dehydration phenomena induced by thermal differences between both the aggregate-matrix as well as cement reactions products as it will be explained later in this paper by using microstructural analysis. On the other hand, the cubic specimens were instrumented with

thermocouples and Figure 9 shows the variation in UPV as both the temperature and the distance from the exposed surface increased. It should be noted that after approximately 110-120 mm the UPV tended to be constant and independent of the temperature applied on the exposed surface. This phenomenon is attributed to the low thermal conductivity of the concrete because after 110 mm (Figure 9), the microstructure of the material was not affected by fire loadings in the same extension as it was on the surface. In Figure 9, it is also noted that UPV decreased drastically near to the face exposed to direct fire (0.0 mm on the X-axis). In Figure 9 each point of the pulse velocity value is the average of six measurements, which were taken in two opposite faces of the cubic specimen as shown in Figure 3.

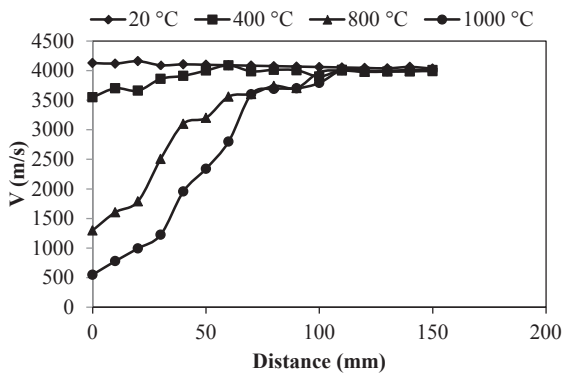

Figure 9 Pulse velocity versus distance from the exposed surface in cubic samples

Relationship between the ultrasonic pulse and porosity

From laboratory tests a regression analysis between the average of six UPVs (V) in m/s and three porosity (P) values in percentage was performed (Table 2), obtaining a correlation coefficient equal to 0.9998 by using a quadratic model (Eq. 6) which was the best fitted model. The p-value was 0.0075, indicating a very strong statistical significance (p-value<0.05) between the variables analyzed. In Table 2 values for T ≥ 600 °C are missing because the experimental samples were disintegrated when they were sunk in water during the performance of the test (section: physical and mechanical tests). Eq. 6 shows increments in the porosity as the temperature was increased (or the UPV decreased). In a similar fashion, Eq. 7 shows the relationship between compressive strength (MPa) and open porosity (%) which followed a quadratic model with r=1.0 and p-value=0.00001. The increment in porosity is attributable to the damage induced in the microstructure by the thermal loadings which promoted the extensive crack development with channel formation, as revealed through microstructural analysis (section: optical microscopy).

Table 2 Porosity tests of concrete samples at elevated temperatures* [13]

T (°C)	H (kg)	D (kg)	S (kg)	P (%)
non-exposed samples	3.98 (0.02)	2.26 (0.02)	4.10 (0.02)	6.120 (0.77)
200	3.85 (0.04)	2.14 (0.02)	4.08 (0.05)	11.84 (0.54)
400	3.82 (0.02)	2.14 (0.01)	4.09 (0.04)	14.19 (0.08)

* All values are the average of three tests. Standard deviation in parenthesis. The H, D and S symbols are defined in Eq. 2.

$$P(V) = -7E^{-6}\ V^2 + 0.0397V - 42.168 \qquad (6)$$

$$C(P) = -0.3846T^2 + 5.5961T + 16.524 \qquad (7)$$

UPV, compressive strength, weight loss and porosity as a function of the temperature

Using the cylindrical specimens a multiple regression analysis model (linear) with the UPV (V in m/s), porosity (P in %) and weight loss (W in %) values as independent variables and the compressive strength (C in MPa) as dependent variable. The investigated temperature range was from 20 to 800 °C and compression values in the upper limit of 1000 °C were not available because of technical reasons as explained above. Eq. 8 shows the complete resulting model

exhibiting a correlation coefficient of 0.9979 with p-value=0.0001.

$$C(V,P,W) = 0.0065V - 1.758P + 0.953W + 21.76 \quad (8)$$

From the sign analysis of the coefficients in Eq. 8, it can be inferred that for two concrete specimens with the same UPV and weight loss, the compressive strength should be higher because of a lower porosity. This result corresponds to fundamental theory of concrete and its relationship with the strength of the material [16]. Then, if the weight loss and porosity values are the same, the compression should be higher in materials with higher UPV measurements. Again, this latter result concurs with other works on the UPV-compressive strength relationship [1,18,20]. Considering that the sign for the weight loss of the coefficient in Eq. 8 is positive, it seems to be wrong at first sight but it may be explained taking into account that increasing the temperature, the higher will be the weight loss but, simultaneously the higher will be the porosity, which exhibited a negative sign. However, the coefficient of the porosity is almost two times the coefficient of the weight loss; therefore the compressive strength will be always a decreasing value.

X-ray diffraction analyses

Table 3 shows the results from the quantitative XRD analyses where the symbol N.Q stands for phases with very low proportions (< 1%), then these phases can be identified but their crystallographic data were not available. At 200 °C the results showed that $C_3A{\cdot}3CaSO_4{\cdot}32H_2O$ (ettringite) and $CaSO_4{\cdot}2H_2O$ (gypsum) vanished when compared to room temperature. Therefore, the water will be evaporated during fire exposure and the chemical compound will be transformed. At 400 °C there is a reduction in the $Al_2Si_2O_5(OH)_4$ and $Ca(OH)_2$ regarding the samples at 200 °C. A reduction on the compressive strength is expected as the microstructure of concrete is deteriorated (higher porosity) when the temperature is increased. This can explain the strength loss detected by the UPV when the fire exposure was increased. At 600 °C the results showed that $Ca(OH)_2$ vanished. This result correlated well with weight loss experienced by the samples (Figure 8) linked to the evaporation of the water molecules. Formation of tensions is expected. This phenomenon explains the micro-crack formation and strength loss exhibited by the samples at that temperature. The chemical compound $Ca_4(Al_8Si_8O_{32})(H_2O)_{16}$ may come from the transformation of $Al_2Si_2O_5(OH)_4$ in conjunction with decomposition of clay materials, where these latter are the source of the calcium. The damage correlates with the visual inspection, optical analyses and compressive strength loss detected with the UPV in previous sections. At 800 °C there was a significant reduction of the $CaCO_3$ (from 15.8% at 600 °C to 3.6% at 800 °C). The reduction can be explained by the decarbonation process of the $CaCO_3$ which generates CaO and the rising of βCa_2SiO_4 and Ca_2SiO_4 from decomposition of clay materials which are products of the cement industry. At 1000 °C results showed a significant reduction in the SiO_2 from 26.6% (T=800 °C) to 17.3% (T=1000 °C). This is expected because an amorphous glass is formed when SiO_2 is exposed to temperatures higher than 870 °C before to the transformation to tridymite. Finally, the amounts of βCa_2SiO_4 and Ca_2SiO_4 increased with respect to the temperature at 800 °C, hence the increased in microstructural damage observed in the optical microscopy section is satisfactory explained. It is also important to note that the increased of βCa_2SiO_4 and Ca_2SiO_4 is owed to calcination process experimented by the $CaCO_3$ when the temperature exceeds 900 °C.

Table 3 XRD summary on concrete samples exposed at different temperatures

Phase	PDF-Card	Quantitative analysis (%)					
		20 °C	200 °C	400 °C	600 °C	800 °C	1000 °C
SiO_2	010-87-2096	33.3	39.6	25.1	29.3	26.6	17.3
$Ca(OH)_2$	000-44-1481	11.1	10.6	8.9	----	----	----
$CaCO_3$	010-72-4582	11.5	10.5	12.3	15.8	3.6	2.5
βCa_2SiO_4	010-83-0462	----	----	----	----	5.9	13.6
Ca_2SiO_4	010-86-0399	----	----	----	----	16.2	19.8
$CaSO_4 \cdot 2H_2O$	000-06-0047	2.0	----	----	----	----	----
$NaAlSi_3O_8$	010-89-6429	----	9.7	7.2	----	9.2	4.6
Ca_2FeAlO_5	010-70-2764	----	----	----	8.0	----	----
$CaAl_2Si_2O_8 \cdot 4H_2O$	000-20-0452	----	----	----	----	N.Q	12.0
$(Mg,Fe)_6(Si,Al)_4O_{10}(OH)_8$	000-29-0701	3.2	7.2	N.Q	N.Q	----	----
TiO_2	010-75-2545	----	N.Q	----	----	----	----
$K_{0.94}Na_{0.06}Al_{0.95}Si_{3\cdot05}O_8$	010-76-0829	4.3	----	----	1.1	----	----
$Al_2Si_2O_5(OH)_4$	000-58-2028	----	3.8	< 1	----	----	----
$KAl_2(Si,Al)_4O_{10}(OH)_2$	000-58-2037	9.4	5.5	5.8	21.6	16.4	9.6
$K_{0.96}Na_{0.04}AlSi_3O_8$	010-83-1895	< 1	< 1	< 1	----	11.1	9.9
$Ca_6Al_2(SO_4)_3(OH)_{12} \cdot 26H_2O$	000-13-0350	1.5	----	----	----	----	----
$Ca_4Al_8Si_8O_{32}(H_2O)_{16}$	010-81-1858	----	----	----	N.Q	----	----
$Na_{0.84}Ca_{0.16}Al_{1.16}Si_{2.84}O_8$	010-76-0927	----	----	----	3.5	----	----
$K_{0.936}Fe_{2.568}Al_{0.504}Al_{1.41}Si_{2.59}O_{10}(OH)_2$	010-74-2574	N.Q	1.7	----	----	N.Q	----
Amorphous	----	18.7	11.2	37.2	20.7	11	10.7

Conclusions

Based on the results of the present experimental work the following conclusions can be made: UPV method showed an excellent performance as an indicator of concrete compressive strength and microstructural states after fire exposure. The experimental results were correlated among physical, mechanical and microstructural properties of concrete exposed to hot environments. Specifically, the weight loss and compressive strength decreased with increasing fire temperature. Whereas, the surface injures, internal damage and porosity increased with increasing fire exposure. Cubic specimens instrumented with thermocouples at different distances from the exposed surface showed significant variations in the UPV conforms both the temperature and the distance was increased. It was noted that after approximately 110-120 mm the UPV tended to be constant and independent of the temperature on the exposed surface. Finally, XRD results showed that ettringite and gypsum disappeared at 200 °C and the amounts of $Ca(OH)_2$ and $CaCO_3$ were reduced when compared to the XRD results at ambient temperature. The reduction of these compounds were associated with severe damage of the concrete microstructure.

References

1. J. Bogas, M. Gomes, A. Gomes. "Compressive strength evaluation of structural lightweight concrete by non-destructive ultrasonic pulse velocity method". *Ultrasonics*. Vol. 53. 2013. pp. 962-972.

2. International Organization for Standardization. *ISO 834-1: 1999. Fire Resistance Tests-Elements of Building Construction.* Standard, International Organization for Standardization (ISO). USA. 1999. pp. 1-25.

3. ASTM International. *ASTM E119-05a. Standard Test Methods for Fire Tests of Building Construction and Materials*. Standard, ASTM International. West Conshohocken, USA. 2005. pp. 1-35.

4. European Committee for Standardization. *EN 1991-1-2 Eurocode 1: Actions on Structures – Part 1-2: General Actions-Actions on Structures Exposed to Fire*. European Standard, European Committee for Standardization. Brussels, Belgium. 2002. pp. 1-61.

5. W. Courge, A. Krom, W. Peleen. "Advanced finite element reliability analysis". *The Structural Engineer*. Vol. 82. 2004. pp. 33-36.

6. C. Eamon, E. Jensen. "Reliability analysis of RC beams exposed to fire". *ASCE Journal of Structural Engineering*. Vol. 139. 2013. pp. 212-230.

7. A. Masood, F. Soltanzadeh, A. Baqui, M. Shariq. *Compressive strength of normal and high strength concrete with polypropylene fibers at elevated temperature.* Proceedings of the International Conference on Advances in Civil, Structural and Environmental Engineering (ACSEE). Zurich, Switzerland. 2013. pp. 37-43.

8. M. Saad, S. Abo, G. Hanna, M. Kotkatat. "Effect of temperature on physical and mechanical properties of concrete containing silica fume". *Cement and Concrete Research*. Vol. 26. 1996. pp. 669-675.

9. L. Phan, N. Carino. "Review of mechanical properties of HSC at elevated temperature". *Journal of Materials in Civil Engineering*. Vol. 10. 1998. pp. 58-64.

10. L. Phan, N. Carino. "Effects of test conditions and mixture proportions on behaviour of high-strength concrete exposed to high temperatures". *ACI Materials Journal*. Vol. 99. 2002. pp. 54-66.

11. ASTM International. *ASTM C470. Standard Specification for Molds for Forming Concrete Tests Cylinders Vertically*. Standard, ASTM International. West Conshohocken, USA. 2008. pp. 1-4.

12. German Institute for Standardization. *DIN EN 206-1:2001-07 [in English]: Concrete – Part 1: Specification, performance, production and conformity.* Stardard, German Institute for Standardization (DIN). Berlin, Germany. 2001. pp. 1-5.

13. J. Ardila, L. Díaz. *Evaluación de las propiedades físicas de concreto sin refuerzo afectado por fuego mediante microscopía óptica y E.N.D*. BSc. Thesis, Universidad Industrial de Santander. Bucaramanga, Colombia. 2013. pp. 1-95.

14. ASTM International. *ASTM C39. Standard Test Method for Compressive Strength of Cylindrical Concrete Specimens*. Standard, ASTM International. West Conshohocken, USA. 2012. pp. 1-7.

15. Instituto Colombiano de Normas Técnicas y Certificación. *NTC 4325. Ingeniería Civil y Arquitectura. Método de ensayo para la determinación de la velocidad del pulso ultrasónico a través del concreto*. Norma Técnica Colombiana, Instituto Colombiano de Normas Técnicas y Certificación (ICONTEC). Bogotá, Colombia. 1997. pp. 1-32.

16. A. Neville. *Properties of Concrete*. 4th ed. Ed. Longman. London, UK. 1995. pp. 844.

17. Z. Guo, X. Shi. *Experiment and Calculation of Reinforced Concrete at Elevated Temperatures*. 1st ed. Ed. Butterworth-Heinemann. Waltham, USA. 2011. pp. 2-16.

18. R. Solís, E. Moreno. "Evaluation of concrete made with crushed limestone aggregate base on ultrasonic pulse velocity". *Construction and Building Materials*. Vol. 22. 2008. pp. 1225-1231.

19. F. Pacheco, J. Castro. "Influence of physical and geometrical properties of granite and limestone aggregates on the durability of a C20/25 strength class concrete". *Construction and Building Materials*. Vol. 20. 2006. pp. 1079-1088.

20. R. Jenkins. "Nondestructive testing – An evaluation tool". *Concrete International*. Vol. 7. 1985. pp. 22-26.

21. E. Whitehurst. *Evaluation of concrete from sonic tests*. American Concrete Institute (ACI) Monograph N.° 2, ACT. Detroit, USA. 1966. pp. 94.

22. Y. Chan, G. Peng, K. Chan. "Comparison between high strength concrete and normal strength concrete subjected to high temperature". *Materials and Structures*. Vol. 29. 1996. pp. 616-619.